antibiotics

MDPI

Article

Hydrological Regime Governs the Fate of Manure-Derived Antibiotic Resistance Genes in Rice–Faba Bean Rotation

Siyi Hu [1,2], Ying Zhang [1,*], Yuanye Zeng [2], Shizhou Shen [2,3], Rui Xin [2], Keqiang Zhang [2,3] and Fengxia Yang [2,3,*]

[1] School of Environmental Science and Engineering, Tianjin University, Tianjin 300350, China; hsy0276@tju.edu.cn
[2] Agro-Environmental Protection Institute, Ministry of Agriculture and Rural Affairs, Tianjin 300191, China; 821012450010@caas.cn (Y.Z.); shenshizhou@caas.cn (S.S.); xinrui@caas.cn (R.X.); zhangkeqiang@caas.cn (K.Z.)
[3] Dali, Yunnan, Agro-Ecosystem, National Observation and Research Station, Dali 671004, China
* Correspondence: yzhang_n@tju.edu.cn (Y.Z.); yangfengxia@caas.cn (F.Y.)

Abstract

Background/Objectives: The proliferation of antibiotic resistance genes (ARGs) in agricultural soils poses a growing One Health threat. However, how hydrological fluctuations in paddy–upland rotations shape the soil resistome remains unclear. This study examined the spatiotemporal dynamics and drivers of soil ARGs in a manure-amended rice–faba bean rotation system. **Methods:** A one-year field experiment was conducted using quantitative PCR and 16S rRNA gene sequencing to characterize ARGs, mobile genetic elements (MGEs), and bacterial communities. **Results:** The hydrological regime and manure application interactively drove resistome succession. Manure introduced diverse ARGs and MGEs, whereas redox fluctuations restructured bacterial host communities and ARG–MGE networks. Compared with the wet phase, the dry phase enriched *intI1* by approximately two orders of magnitude. Specifically, the log10-transformed *intI1*/16S rRNA gene copy-number ratio increased from −7.11 to −5.14, indicating greater potential for horizontal gene transfer. The fallow transition period represented a critical resistome-restructuring stage with lasting legacy effects. Structural equation modeling identified a dominant carbon–microbe–MGE cascade. Active organic carbon fractions, including dissolved organic carbon (DOC) and readily oxidizable carbon (ROC), shaped microbial community structure, which regulated MGE abundance and ultimately ARG dynamics. MGEs were the strongest direct driver of ARGs (path coefficient = 0.575, $p < 0.001$). **Conclusions:** Wet–dry alternation modulates soil resistance risks through the carbon–microbe–MGE cascade. The fallow transition period therefore provides a key target for managing hydrology and carbon inputs to mitigate ARG dissemination in sustainable agroecosystems.

Keywords: antibiotic resistance genes; paddy–upland rotation; manure application; microbial community succession; organic carbon fractions

Check for updates

Academic Editor: Helena Felgueiras

Received: 21 September 2026
Revised: 17 October 2026
Accepted: 21 October 2026
Published: 23 October 2026

Copyright: © 2026 by the authors. Licensee MDPI, Basel, Switzerland. This article is an open access article distributed under the terms and conditions of the Creative Commons Attribution (CC BY) license.

1. Introduction

Antibiotic resistance genes (ARGs) have emerged as persistent environmental contaminants, presenting a major threat to global public health under the "One Health" framework [1]. Intensive antibiotic use in livestock and crop production has made agricultural soils major reservoirs of ARGs [1,2]. Beyond persisting in microbial communities via vertical inheritance, ARGs can, more critically, transfer across species barriers through horizontal gene transfer (HGT) mediated by mobile genetic elements (MGEs) [3]. Agricultural soils

provide an important interface where ARGs can circulate among environmental, commensal and potentially pathogenic bacteria. Manure application and wastewater irrigation are major routes by which exogenous ARGs enter topsoil [4,5]. Once established, these genes can reach edible crop tissues through rhizosphere and phyllosphere pathways [6,7]. Contaminated produce, irrigation water and occupational contact may then facilitate their entry into human-associated microbial communities. Such transmission can expand the reservoir of clinically relevant resistance genes and may ultimately undermine antibiotic efficacy, with consequences for human health [8]. Accordingly, suppressing the enrichment and trophic propagation of soil ARGs has become an urgent research priority in agroecology.

Current mitigation strategies for soil ARG pollution primarily rely on physicochemical remediation (e.g., biochar adsorption, advanced oxidation processes) and agro-ecological management measures [9]. Because large-scale physical remediation is often economically impractical, modulating the soil microenvironment through optimized cropping patterns offers a more sustainable alternative to suppress antibiotic-resistant bacteria (ARB) and inhibit ARG expression. ARB represent the major biological carriers of ARGs and can facilitate resistance propagation through clonal expansion and horizontal gene transfer. In agricultural environments, manure-amended soils frequently harbor clinically relevant ARB, including *Escherichia coli*, *Klebsiella pneumoniae*, *Enterococcus* spp., and *Staphylococcus aureus*, which may carry transferable resistance determinants associated with β-lactams, tetracyclines, macrolides, and aminoglycosides [10,11]. Environmental reservoirs of such ARB increase the risk of resistance transfer to human pathogens, contributing to the growing global burden of antimicrobial resistance that threatens clinical infection treatment [12]. Existing studies indicate that rational fertilization, water management, and crop diversification can alter soil properties (e.g., pH, organic matter) and microbial community structures, thereby influencing ARG profiles [13–15]. Specifically, crop rotation—a classical conservation tillage practice—has been shown to enhance soil health; however, specific mechanisms governing the soil antibiotic resistome remain inadequately understood [16].

Existing studies on ARGs in cropping systems predominantly focus on continuous cropping obstacles or exogenous inputs from organic fertilizer application. Distinct root exudates from different crops are known to reshape the rhizosphere microbiota and exert selective pressures on ARGs [17,18]. For instance, the legume–rhizobia symbiotic system may alter microbial taxa associated with the soil nitrogen cycle, indirectly affecting ARG host distribution [19]. However, most findings are derived from dryland rotation systems. In contrast, the unique ecological niche of paddy–upland rotation remains underexplored. These systems impose cyclical stresses characterized by drastic fluctuations in redox potential (Eh), flooded–non-flooded cycles, and the succession of aerobic and anaerobic microbial communities. These hydrological oscillations are highly likely to fundamentally reorganize ARG dynamics by modulating MGE activity and HGT potential, yet the underlying evolutionary mechanisms remain unelucidated [20,21].

Rice–faba bean rotation represents a typical paddy–upland cropping system in China, and integrates flooded rice with dryland legume cultivation, forming a unique Water–Dry and Carbon–Nitrogen coupled environment [22]. This system likely creates a dynamic ecological filter, where alternating redox conditions and organic carbon availability interact with manure inputs to selectively shape microbial hosts and ARG transfer networks [23]. Yet, few studies have delineated the spatiotemporal dynamics of soil ARGs across different growth seasons under this specific rotation, or elucidated the mechanistic pathways linking environmental factors to resistome assembly. These knowledge gaps constrain our ability to proactively control agricultural non-point source ARG pollution via optimized cropping systems.

To fill these research gaps, we conducted a field plot experiment with manure fertilization and rice–faba bean rotation treatments. This study aims to address three core scientific questions: (1) to comprehensively characterize the spatiotemporal variation patterns of soil ARGs across cyclic dry-wet hydrological transitions; (2) to identify the key environmental drivers, with a specific focus on the interactive effects between active organic carbon fractions and seasonal hydrological regimes; and (3) to elucidate the microbial co-occurrence networks and host succession mechanisms mediating the persistence and horizontal dissemination of ARGs in manured soil. Collectively, this work clarifies the complete ecological blueprint describing how paddy–upland alternations modify soil antibiotic resistance risks, and provides theoretical support for sustainable, resistance-mitigating agricultural management.

2. Materials and Methods

2.1. Experimental Site and Raw Materials

This long-term field trial was conducted at the Yunnan Dali Agro-Ecosystem National Field Observation and Research Station, located in Xizhou Town, Dali Bai Autonomous Prefecture, Yunnan Province (100°10′ E, 25°53′ N). The experimental site is the Erhai Lake basin at an altitude of 1980 m, featuring a subtropical monsoon climate. The multi-year average annual temperature reaches 14.6 °C, with annual precipitation of 1048 mm and average relative humidity of 66%. The native soil at the experimental plots is classified as dark brown soil, with baseline physicochemical parameters summarized in Table 1. Cattle manure was applied as the organic fertilizer, replacing 30% of the chemical nitrogen fertilizer input (approximately 30 kg per individual plot). The cattle manure had an organic matter content of 35% (350 g/kg, dry basis) and a pH of 7.5, with TN, TP, and TK contents of 1.92% (19.2 g/kg), 1.92% (19.2 g/kg), and 1.10% (11.0 g/kg), respectively. The rice cultivar was early-maturing japonica hybrid Yunjing 26 (*Oryza sativa* L.), while the faba bean cultivar was medium-maturing variety Fengdou 7 (*Vicia faba* L.).

Table 1. Physicochemical properties of initial soil.

Index	Initial Soil
SOC (g/kg)	23.36
MAOC (g/kg)	12.37
ROC (mg/kg)	1782.07
DOC (mg/kg)	117.69
pH	6.3
TP (g/kg)	0.650
OM (g/kg)	40.27

2.2. Experiment Design

The field experiment consisted of four distinct treatments with three biological replicates per treatment, generating 12 independent plots (4 m × 5 m each): (i) control with no manure input and no crop planting (CU), (ii) crop rotation without manure input (CP), (iii) manure application without crop planting (MU), and (iv) manure application combined with crop rotation (MP). These 12 plots were repeatedly sampled across nine time points (designated P1–P9), representing repeated measures of the same experimental units. All plots were subjected to the same hydrological management throughout the experiment and established on farmland with no prior history of organic fertilizer application. Manure was applied once as basal fertilizer prior to rice sowing. Rice seeds were pre-germinated and directly sown, while faba bean seeds were surface-sterilized in 1% sodium hypochlorite for 10 min before sowing. Sampling dates, soil moisture content (SMC), oxidation–reduction

potential (ORP) and floodwater depth are detailed in Table 2. To systematically characterize how ARGs respond to cyclic hydrological transitions, the annual rotation was divided into four phases according to crop and water management: pre-planting basal fertilization (P1), continuous flooded rice cultivation (P2–P4), fallow transition period (P5), and aerobic upland faba bean growth (P6–P9). Soil samples were collected from the 0–20 cm topsoil layer, which represents the primary zone influenced by crop root activity and agricultural management practices. At each plot, five subsamples were collected using a five-point sampling method and mixed into a composite sample. Approximately 1 kg of the composite sample was retained by quartering and stored at −20 °C until DNA extraction.

Table 2. Sampling times, corresponding growth stages and hydrological conditions in the rice–faba bean rotation system.

Sampling Code	Growth Stage	Sampling Date	SMC (%)	Floodwater Depth (cm)	ORP (mV)
P1	After fertilization	12 June 2024	22.7		198
P2	Rice tillering stage	12 July 2024	–	3	−96
P3	Rice jointing stage	16 August 2024	–	3	−103
P4	Rice grain filling stage	28 August 2024	–	3	−88
P5	Fallow period (post-rice)	19 October 2024	34.7	–	257
P6	Faba bean seedling stage	20 January 2025	33.2	–	232
P7	Faba bean flowering stage	20 February 2025	25.8	–	239
P8	Faba bean pod-setting stage	20 March 2025	25.5	–	241
P9	Faba bean harvest stage	20 April 2025	22.7	–	228

2.3. Determination of Soil Properties

Soil pH was measured via the potentiometric method [24]. Soil organic carbon (SOC) was determined by dichromate ($K_2Cr_2O_7$) oxidation with external heating [25]. Readily oxidizable carbon (ROC) was measured by the potassium permanganate oxidation method [26]. Dissolved organic carbon (DOC) was extracted and analyzed using a total organic carbon analyzer [27]. Sucrase activity and β-glucosidase activity were assayed by the 3,5-dinitrosalicylic acid (DNS) and p-nitrophenyl-β-D-glucopyranoside (PNPG) colorimetric methods, respectively [28,29]. Chloride ion (Cl^-) was measured by silver nitrate titration and magnesium ion (Mg^{2+}) by atomic absorption spectrometry (AAS) [30]. Total phosphorus (TP) was determined by $HClO_4$–H_2SO_4 digestion [31]; inorganic phosphorus (IP) and organic phosphorus (OP) were extracted with 1 mol·L^{-1} HCl and quantified by the molybdenum–antimony colorimetric and ignition methods, respectively [32]. All measurements were performed in triplicate.

2.4. Soil DNA Extraction and Quality Control

For each soil sample, 0.5 g of fresh soil was used for genomic DNA extraction, with three technical replicates per sample. Total genomic DNA was extracted using the FastDNA SPIN Kit for Soil (MP Biomedicals, LLC, Santa Ana, CA, USA) following the manufacturer's instructions, with a final elution volume of 70 µL. DNA quality was assessed by 1.0% agarose gel electrophoresis, and DNA concentration was quantified using a Nano Drop 2000 spectrophotometer (Thermo Scientific, Wilmington, DE, USA). The A260/A280 ratios of extracted DNA were approximately 1.8, indicating high DNA purity. Extracted DNA was preserved at −20 °C for downstream molecular quantification and sequencing analysis.

2.5. Real-Time Quantitative PCR (qPCR) of Target Functional Genes

In total, 25 target functional genes covering eight major antibiotic resistance categories and three MGE markers (the integron-integrase genes *intI1* and *intI2*, and the conjugative

transfer gene *traA*) were selected for absolute qPCR quantification based on their wide distribution and high health risks in agricultural soils: sulfonamide resistance genes (*sul*-ARGs: *sul1*, *sul2*), tetracyclines (*tet*-ARGs: *tetO*, *tetL*, *tetW*, *tetQ*, *tetM*, *tetX*), β-lactams (*bla*-ARGs: $bla_{\text{OXA-1}}$, bla_{ampC}, $bla_{\text{TEM-1}}$, $bla_{\text{NDM-1}}$), quinolones (*qnrA*, *qnrB*, *qnrS*, *oqxB*), macrolides (*ermB*), aminoglycosides (*strA*, *strB*), phenicols (*cfr*, *fexA*), polymyxins (*mcr-1*), conjugative transfer (*traA*), and integrons (*intI1*, *intI2*). In addition to the target genes, the bacterial 16S rRNA gene was quantified by qPCR as the normalization reference. All qPCR amplification assays were performed on an Applied Biosystems 7500 Real-Time PCR platform using nuclease-free 96-well reaction plates. Detailed qPCR reaction systems, thermal cycling programs and primer sequences are provided in Supplementary Text S1 and Table S1. Standard amplification curves with efficiency ranging from 90% to 110% and coefficient of determination (R^2) $\geq$ 0.99 were retained for subsequent gene abundance calculation.

2.6. 16 S rRNA Gene Sequencing

Extracted soil DNA samples were submitted to Shanghai Personal Biotechnology Co., Ltd. (Shanghai, China) for bacterial 16S rRNA gene amplicon sequencing. The V3–V4 hypervariable region of the bacterial 16S rRNA gene was amplified using the primer pair 338F (5′-barcode+ACTCCTACGGGAGGCAGCA-3′) and 806R (5′-GGACTACHVGGGTWTCTAAT-3′), with unique 7–10 bp barcode sequences incorporated into the forward primers to distinguish samples within the same sequencing library [33]. Sequence analysis was performed using QIIME2 (version 2024.5) following the official workflow [34]. Raw sequence data were demultiplexed using the demux plugin, and primer sequences were removed using the cutadapt plugin [35]. The resulting sequences were quality filtered, denoised, merged, and chimera-filtered using DADA2 [36] to generate amplicon sequence variants (ASVs). Taxonomic assignment of ASVs was performed using the naïve Bayes classifier implemented in the q2-feature-classifier plugin [37] against the SILVA release 138.1 database [38].

2.7. Bioinformatic and Statistical Analysis

To account for repeated measurements across nine sampling periods, ARG and MGE abundances were analyzed using repeated-measures linear mixed-effects models implemented with the nlme package (v3.1.168), with manure amendment, planting, sampling period, and their interactions as fixed effects and plot identity as the repeated-measure subject. A first-order autoregressive [AR(1)] correlation structure was used to account for within-plot temporal dependence. Post hoc comparisons were performed using the emmeans package (v2.0.4). Absolute abundance was expressed as gene copies per gram of dry soil, whereas relative abundance was calculated as target-gene copies divided by 16S rRNA gene copies. The gene abundance data were log10-transformed before model fitting. Model residuals were examined for normality and homoscedasticity. For multiple comparisons, p values were adjusted using the Benjamini–Hochberg false discovery rate (FDR) procedure, with $q < 0.05$ considered significant. Pearson and Spearman correlations were calculated using the R stats package (v4.5.2). Redundancy analysis (RDA), Mantel tests, Bray–Curtis dissimilarities, and PERMANOVA were performed using the vegan package (v2.7.3), while principal coordinate analysis (PCoA) was conducted using the ape package (v5.8.1). Co-occurrence networks were constructed based on Spearman correlation analysis using the Hmisc package (v5.2.5) in R, with data preprocessing and network table preparation performed using the tidyverse package (v2.0.0). Networks were generated among ARGs, MGEs, and bacterial genera with mean relative abundances > 0.01%. Each treatment contributed nine observations during the rice season (three plots sampled at three periods) and 12 during the faba bean season (three plots sampled at four periods).

Given the greater variability of correlation estimates in the smaller rice season dataset, a more stringent correlation cutoff was applied: retaining associations with $p < 0.05$ and $|\rho| > 0.90$ for rice or $p < 0.05$ and $|\rho| > 0.80$ for faba bean. The resulting networks were visualized using Gephi v0.10.1. Partial least squares structural equation modeling (PLS-SEM) was performed using the R plspm package (v0.6.0) to evaluate direct and indirect relationships among environmental variables, microbial communities, MGEs, and ARGs. Data visualization was performed using the R ggplot2 package (v4.0.1). All analyses were conducted in R (v4.5.2).

3. Results and Discussion

3.1. Interactive Effects of Hydrological Regime and Manure Amendment on Soil Resistome Structure

In the present study, the specified 22 ARG types (i.e., *sul1*, *sul2*, *qnrA*, *qnrB*, *qnrS*, *oqxB*, *tetL*, *tetM*, *tetO*, *tetQ*, *tetW*, *tetX*, *ermB*, *strA*, *strB*, *mcr-1*, *fexA*, *cfr*, $bla_{\text{OXA-1}}$, $bla_{\text{TEM-1}}$, $bla_{\text{NDM-1}}$ and bla_{ampC}) and three MGE-related targets (i.e., *intI1*, *intI2* and *traA*) were all detected and tracked in soils under the rice–faba bean rotation across the full rotation cycle. Most ARGs were widely distributed, with 19 detected in all 108 samples and *oqxB*, $bla_{\text{TEM-1}}$ and *tetM* detected in 98.1%, 91.7% and 83.3% of samples, respectively (Figure 1a). Among them, *sul*-ARGs were the most abundant gene category, averaging 1.40×10^{-3} copies per 16S rRNA gene, which is consistent with previous reports [39], followed by *tet*-ARGs with an average abundance of 7.98×10^{-5} copies per 16S rRNA gene, primarily represented by *tetO* and *tetL*. Of particular concern was that *bla* genes, the subtype closely related to human health, were less abundant across the rotation cycle, with an average abundance of 1.24×10^{-5} copies per 16S rRNA gene copy. All samples also contained the three MGEs, with *intI1* occurring at the highest mean abundance. Manure amendment altered this background within the first sampling period. At P1, total ARG abundance in MU and MP was 4.1- and 7.7-fold higher than in CU, respectively, shifting both treatments away from the unamended soils in the PCoA ordination (Figure 1b,c). PCoA1 and PCoA2 captured 51.7% and 10.6% of compositional variation, while the AR(1) model retained a strong manure effect after FDR correction ($q = 2.48 \times 10^{-4}$) (Figure 1a). At the gene level, manure affected 13 ARGs spanning six resistance classes, including *sul1*, *sul2*, *tetL*, *tetQ*, *tetW*, *tetX*, $bla_{\text{OXA-1}}$, *strA*, *strB*, *fexA*, *cfr*, *ermB* and *mcr-1* ($q < 0.05$). Among the MGEs, only *intI1* showed a significant manure main effect ($q = 4.00 \times 10^{-4}$). Most gene responses were period-dependent: period × manure interactions affected 22 of the 25 targets, and three-way interactions among time, manure and planting remained significant for 20 targets. Similar field experiments have recorded rapid ARG enrichment after manure application [40], and global metagenomic evidence connects organic fertilization with greater diversity of genetically linked resistance determinants [41].

The manure pulse did not persist uniformly through the rotation. Total ARG abundance fell sharply between P1 and P2, remained relatively stable during rice growth, rebounded at the P5 fallow transition and declined again during the faba bean phase (Figure 1c). Planting altered this trajectory through both the period × planting interaction ($q = 0.0039$) and the period × manure × planting interaction ($q = 0.0053$), pointing to crop development as a filter on the manure-enriched resistome. Flooding duration, redox change and dry–wet transitions can drive comparable turnover in paddy-soil ARG profiles [42]. The behavior of *intI1* added a mobility-related dimension to this temporal pattern. Total ARG abundance tracked *intI1* closely after manure application ($\rho = 0.85$, $p = 0.00042$, $n = 12$) and more moderately during rice growth ($\rho = 0.43$, $p = 0.0083$, $n = 36$; Figure 1d). This coupling disappeared during fallow ($\rho = -0.22$, $p = 0.48$, $n = 12$) and faba bean growth ($\rho = -0.11$, $p = 0.45$, $n = 48$), suggesting that manure initially ampli-

fied integron-associated dissemination potential before rotation-related environmental filtering weakened the ARG–*intI1* relationship. Manure and flooding have been shown to strengthen ARG–MGE associations in paddy soil–water systems [15], while soil moisture and plant presence can modulate resistome–MGE connectivity [43]. The central transition was therefore not merely a decline in ARG abundance, but a shift from a manure-linked ARG–*intI1* assemblage to a later resistome increasingly filtered by crop stage and associated hydrological conditions.

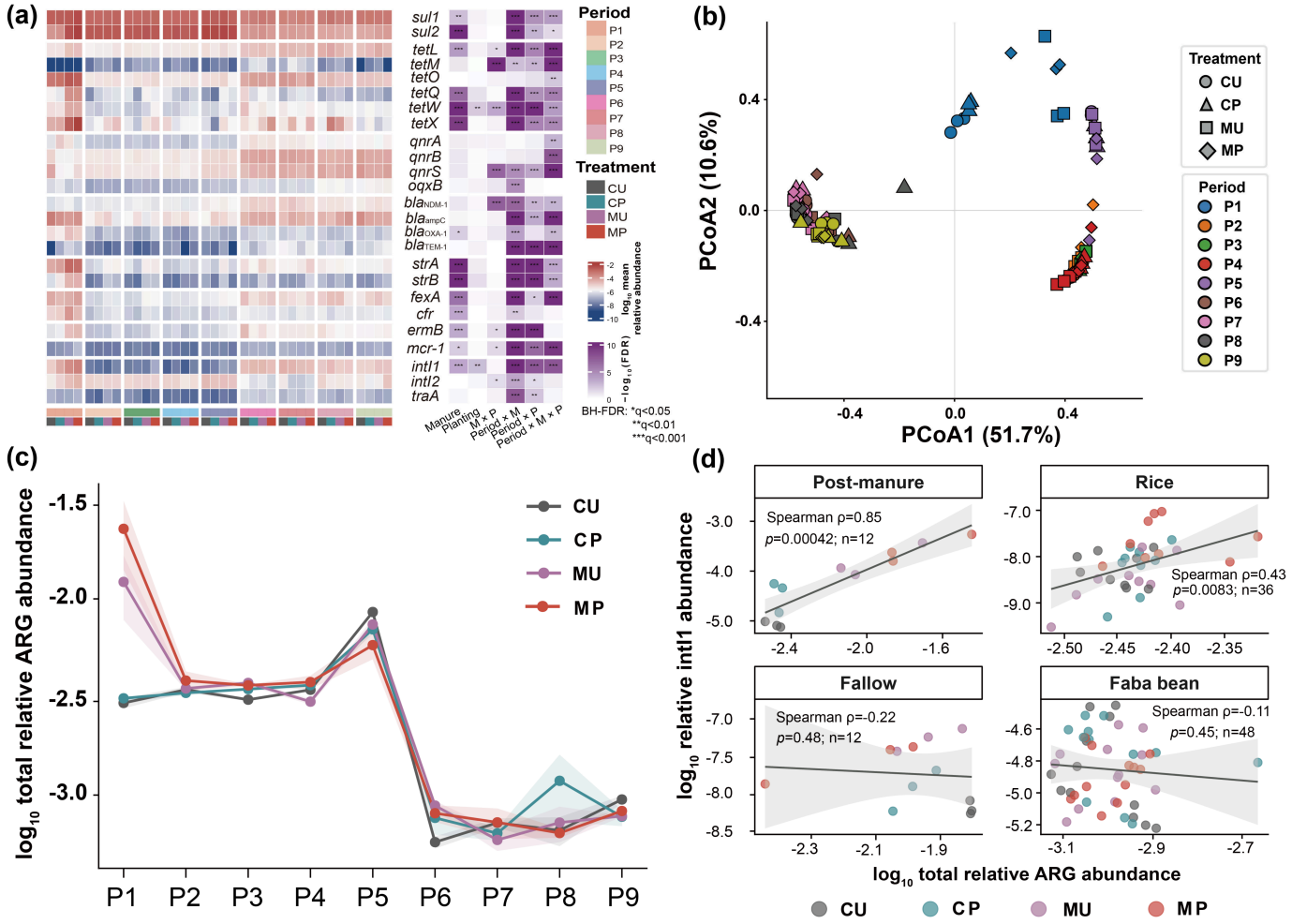


Figure 1. Spatiotemporal dynamics of ARGs under different management practices. (**a**) Heatmap showing the $\log_{10}$-transformed relative abundances of all ARGs and MGEs, with the adjacent matrix indicating $-\log_{10}$ (FDR-adjusted *p* values) for treatment and interaction effects. (**b**) PCoA of ARG composition. (**c**) Temporal changes in $\log_{10}$-transformed total ARG relative abundance under CU, CP, MU and MP treatments. (**d**) Stage-specific correlations between ARGs and MGEs, with Spearman's ρ and *p* values indicated.

3.2. Temporal Succession of Typical ARGs Driven by Rice–Faba Bean Rotation

ARG variability differed markedly among genes, with coefficients of variation (CVs) ranging from 0.53 to 2.68 (Figure 2a). Based on the core/variable resistome analytical framework proposed by [44], *qnrB* and *tetL* were classified as core resistome members, featuring detection frequency > 80%, relative abundance > 10^{-6} and CV < 0.70. Their persistence across all four phases formed a stable background against which more responsive genes could be distinguished. In contrast, genes including *strA*, *strB*, *tetX*, *tetQ*, and *tetO* displayed high CV values and were categorized as variable resistome components. These variable ARGs are frequently carried on plasmids and associated with diverse MGEs,

and their drastic abundance fluctuations were tightly coupled with redox shifts during flood-drainage transitions. Other target genes including *cfr*, *fexA*, and quinolone resistance subtypes (*qnrS*, *qnrB*, *qnrA*) maintained relatively stable concentrations, with abundance variations restricted within one order of magnitude across all sampling timepoints.

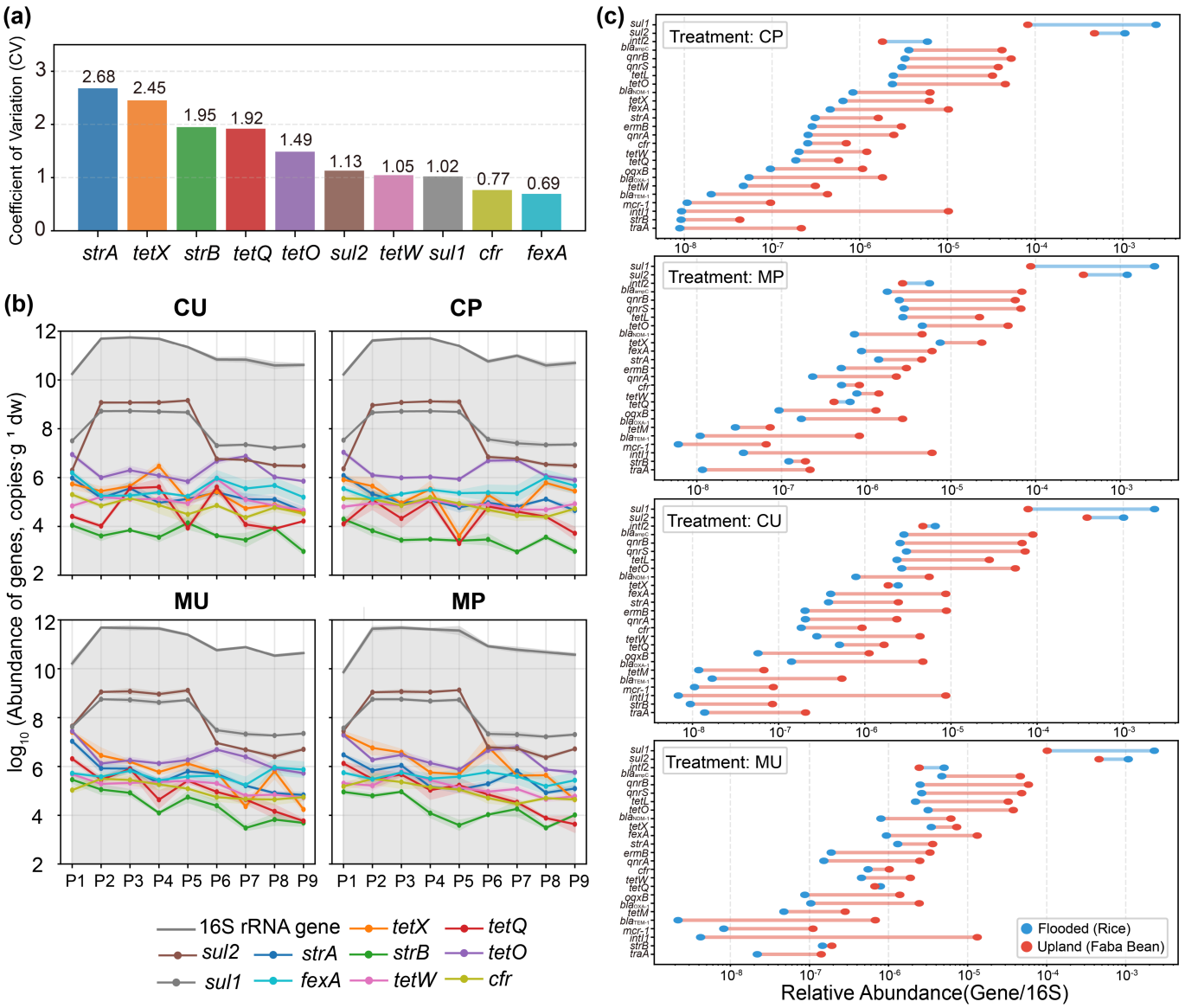


Figure 2. Temporal dynamics and variation characteristics of antibiotic resistance genes (ARGs) across the nine crop rotation periods. (**a**) The top 10 ARGs with the highest coefficient of variation (CV) across all nine periods, representing the most temporally dynamic resistance genes in the rotation system. (**b**) Dynamic changes in the absolute abundance of the top 10 highly variable ARGs identified in (**a**) over time. The semi-transparent shaded areas along each line represent the standard deviation (SD) of the replicates. The gray shaded background area illustrates the absolute abundance of the bacterial 16S rRNA gene. (**c**) Dumbbell plot comparing the shifts in the average relative abundance of all detected ARGs between the rice rotation stage (blue) and the faba bean rotation stage (red).

ARG abundance displayed clear phase-dependent fluctuations throughout the rotation cycle, with the fallow transition stage (P5) identified as the critical resistome remodeling window (Figure 2b). During the early rotation and rice phase, total ARG abundance remained high and stable across all four treatments. For instance, the dominant gene *sul2* maintained average absolute abundances of $(1.47 \pm 0.32) \times 10^9$, $(1.21 \pm 0.28) \times 10^9$, $(4.82 \pm 1.15) \times 10^8$, and $(5.37 \pm 0.89) \times 10^8$ copies·g^{-1} dry soil in CU, CP, MU and MP plots,

respectively, with intra-treatment CV values below 0.25. Similarly, *tetQ* and *sul1* persisted at 10^8 and 10^7 copies·g^{-1} dry soil levels, with abundance fluctuations limited to less than 0.5 orders of magnitude. This remarkable stability under continuous anaerobic flooding indicates that stochastic ecological drift and random dispersal dominated short-term resistome turnover within homogeneous anoxic soil environments. Upon entering the fallow transition phase (P5), soil drainage triggered synchronous declines and comprehensive restructuring of total ARG pools, accompanied by rapid reassembly of the overall soil microbial community [45]. Following the fallow period, ARG abundance gradually reached a new equilibrium during aerobic faba bean cultivation. This change was accompanied by a shift in the microbial community from anaerobes to aerobes and facultative anaerobes, greater divergence among treatments, and stronger deterministic selection.

The shift from flooded anaerobic to aerobic upland conditions induced system-wide expansion of soil resistome diversity and abundance (Figure 2c). Following soil drainage and faba bean sowing, most ARGs increased markedly in relative abundance, demonstrating that aerobic soil microhabitats and legume rhizosphere effects facilitate the proliferation of diverse ARG-carrying microbial taxa. The faba bean upland phase therefore represents a critical window for resistome resurgence rather than attenuation, a pattern primarily driven by activated aerobic metabolic pathways and elevated MGE-associated dissemination potential mediated by upregulated MGEs. Overall, the temporal succession of soil ARGs is not linear but a stepwise restructuring coupled with water regime transitions. The fallow transition (P5) acted as a sharp turning point, triggering rapid microbial turnover and niche reallocation [46], generating a legacy effect that shaped ARG distribution in the subsequent dry season. These results highlight the fallow transition window as a key intervention target to control antibiotic resistance dissemination in paddy–upland rotation agroecosystems.

3.3. Microbial Community Assembly and Succession Under Cyclic Flooded–Non-Flooded Regimes

Soil microbial communities, as the primary hosts and vectors for ARGs, directly influence ARG fate through shifts in composition and structure [47]. The MP treatment underwent marked microbial turnover across the annual rotation (Figure 3a,b), whereas the corresponding phylum- and genus-level community profiles for all four treatments are presented in Supplementary Figures S1–S3. At the phylum level, Actinomycetota—well-documented as prolific antibiotic producers and key reservoirs of intrinsic ARGs [48]—dominated the community across all phases yet declined from 42.77% at P1 to 31.55% at P9, suggesting a gradual reduction in the background pool of endogenous ARGs. Meanwhile, the relative abundances of Chloroflexota (+12.5%), Acidobacteriota (+24.8%), and Pseudomonadota (+17.0%) increased continuously, indicating that flooded–non-flooded alternation systematically favored the enrichment of these phyla. A core microbiome of 119 bacterial genera persisted across the entire rotation (Figure 3c), forming a conserved framework that likely serves as a stable endogenous reservoir for the resistome and buffers against strong physicochemical fluctuations. In contrast, the accessory microbiome exhibited high temporal plasticity (Figure 3d), with gradual taxonomic turnover between consecutive stages, reflecting stepwise community restructuring. The appearance of stage-restricted genera after drainage points to strong filtering during the transition from anaerobic to aerobic soil.



Figure 3. Taxonomic composition, core microbiome distribution, and overall diversity of the microbial community in the MP treatment across nine rotation periods. (**a**,**b**) Relative abundance of the top 20 bacterial phyla (**a**) and genera (**b**) over time. (**c**) Flower plot displaying the number of core (shared across all periods) and unique bacterial genera. (**d**) UpSet plot detailing the complex intersections of shared bacterial genera across the nine periods. Only the top 20 largest intersections ranked by the number of shared genera are displayed. (Note: Only genera with > 0.01% relative abundance were included in (**c**,**d**)). (**e**) Alpha diversity indices (Chao1, Shannon, and Observed features) showing the temporal shifts in species richness and evenness. (**f**) PCoA based on genus-level relative abundance, illustrating the clustering and structural successions of the microbial communities.

A striking transient dynamic was observed for Bacillota, which increased by over 221% during the flooded rice season (peaking at P3) and then declined sharply during

the fallow period (P5). This pattern is consistent with the short-term enrichment of ARGs in manured soil under flooded conditions [49], indicating that anaerobic conditions temporarily promote gut-associated bacteria such as *Bacillus* and *Clostridium*, which frequently carry clinically important ARGs. In contrast, Pseudomonadota, a major host phylum for ARGs [50], increased gradually from 16.76% at P1 to 19.61% at P9, with a peak of 22.02% at P8. As key carriers involved in plasmid-mediated horizontal ARG transfer [51], the sustained increase in Pseudomonadota carries important implications for ARG dynamics. Microbial richness and diversity also increased after flooding ended, with Chao1, Shannon diversity and observed features showing inflection points at P4 and P6 (Figure 3e). This elevation was closely linked to the rapid growth of rare taxa such as *SC-I-84* and *Vicinamibacterales* during the faba bean season, likely supported by rhizosphere effects and nitrogen fixation that create specialized niches [52]. This diversity pattern represents a unique advantage of rice–faba bean rotation, differing markedly from the diversity reduction commonly observed under monocropping [53].

Beta-diversity analysis further validated that seasonal hydrological regime, rather than manure fertilization or crop planting, constituted the dominant driver structuring overall soil microbial assemblages. PCoA was performed using Bray–Curtis dissimilarity based on genus-level relative abundance (Figure 3f). The first two axes explained 51.0% and 6.4% of the variation, respectively. Samples clustered tightly by rotation phase, with clear separation among pre-planting, flooding, and dry-farming stages. Permutational multivariate analysis of variance (PERMANOVA) revealed that period, treatment, and their interaction were significantly associated with community composition (period: $R^2 = 0.767$; treatment: $R^2 = 0.047$; interaction: $R^2 = 0.128$; all $p \leq 0.0001$, 9999 permutations). Collectively, these results demonstrate that flooded–non-flooded alternation acts as a powerful ecological filter that sequentially selects distinct microbial hosts and steers the succession of the soil resistome. The transient bloom of Bacillota under flooding, the continuous increase in Pseudomonadota, and the overall enhancement of microbial diversity jointly reshape the host landscape for ARGs, thereby regulating the persistence, transmission, and ecological risk of soil antibiotic resistance in paddy–upland rotation systems.

3.4. Co-Occurrence Patterns of ARGs, MGEs, and Bacterial Communities Across Rotation Stages and Manure Treatments

Co-occurrence network analysis was used to explore potential associations between ARGs and bacterial taxa under different rotation stages and manure treatments (Figure 4; Table 3). During flooded rice cultivation, the CP network comprised 123 nodes (21 ARGs, 3 MGEs, and 99 genera) and 135 edges, while manure application (MP) expanded the network to 154 nodes (20 ARGs, 3 MGEs, and 131 genera) with 167 edges, indicating enhanced ARG–microbe connectivity under manure input. After transitioning to the faba bean season, network size decreased in CP (81 nodes, 141 edges) but remained larger in MP (117 nodes, 164 edges), suggesting that manure-amended soil maintained a broader ARG–taxon association network following the transition from rice to faba bean cultivation. Modularity analysis further demonstrated fundamental structural differences between flooded and upland phases: rice networks exhibited higher modularity (0.743–0.814) with 14–17 modules, whereas faba bean networks showed lower modularity (0.571–0.675) with fewer but more interconnected modules (7–8). These patterns indicate that anaerobic flooding promotes compartmentalized ARG–host associations and niche specialization, while aerobic upland conditions enhance cross-taxa connectivity and may facilitate horizontal gene transfer [54]. Thus, water regime acted as the primary driver of ARG network reorganization [55].

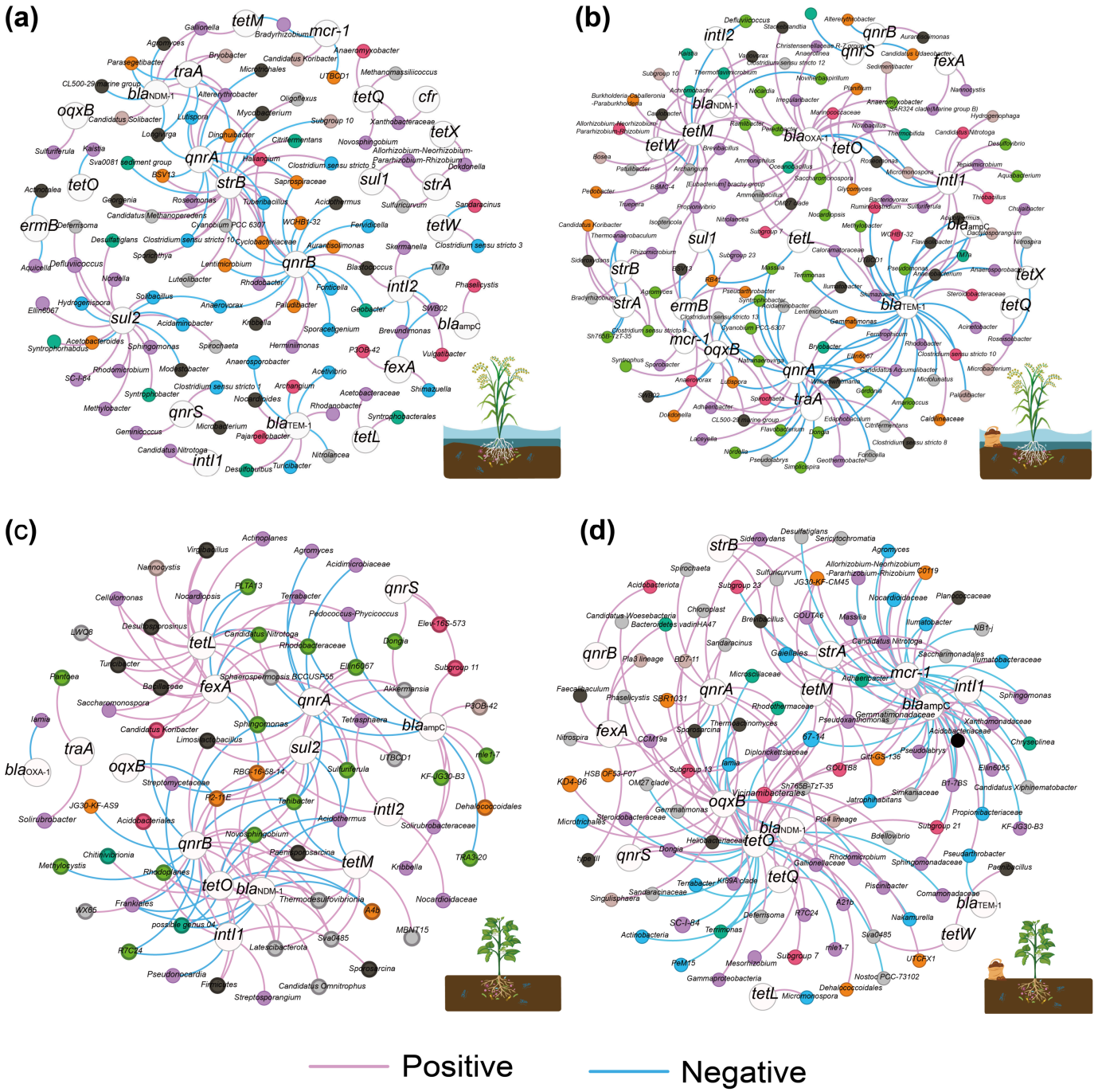


Figure 4. Co-occurrence network analysis between ARGs and bacterial genera across different crop and fertilization treatments. Network diagrams illustrating the complex co-occurrence patterns of ARGs/MGEs and bacterial taxa (at the genus level) under four treatments: (**a**) flooded rice without manure, (**b**) flooded rice with manure, (**c**) upland faba bean without manure, and (**d**) upland faba bean with manure. The nodes represent specific ARGs, MGEs, and bacterial genera. The connecting edges denote significant correlations between them, with pink lines indicating positive correlations and blue lines indicating negative correlations.

Table 3. Global topological properties of ARG-microbial co-occurrence networks.

Crop	Treatment	Nodes	Edges	Density	Modularity	Communities
Rice	CP	123	135	0.018	0.743	17
	MP	154	167	0.014	0.814	14
Faba bean	CP	81	141	0.044	0.571	7
	MP	117	164	0.024	0.675	8

The ARGs occupying central network positions also changed with season and manure input. During the rice season, *strB* and *qnrB* were hubs in CP, whereas $bla_{\text{TEM-1}}$, $bla_{\text{OXA-1}}$ and *tetM* became prominent in MP. Notably, $bla_{\text{OXA-1}}$ formed extensive connections only under flooded and manured conditions, showing strong positive correlations with Bacillota and Actinomycetota genera (e.g., *Christensenellaceae R-7* group, *Novibacillus*, and *Glycomyces*) frequently associated with manure inputs [56]. During the faba bean season, *tetL*, *tetO* and *fexA* occupied central positions in CP, while bla_{ampC} and *mcr-1* emerged as hubs in MP. Importantly, *mcr-1* was undetectable in CP networks but formed extensive associations under manure amendment, a concerning observation given colistin's role as a last-resort antibiotic [57].

Putative ARG–taxon associations were also partitioned by hydrological phase (Figure 5a,b). Key genes such as *tetX* and $bla_{\text{OXA-1}}$ were associated with bacterial taxa only during the flooded rice season, with $bla_{\text{OXA-1}}$ linked to manure-associated taxa. In contrast, the high-risk gene $bla_{\text{NDM-1}}$ exhibited strong host plasticity, shifting hosts across rotation phases and fertilization regimes. Integron dynamics further illustrated seasonal reorganization of horizontal gene transfer pathways: manure strengthened *intI1* associations with anaerobic taxa during flooding [58], while hosts shifted to aerobic Actinomycetota and Pseudomonadota under upland conditions. *Candidatus Nitrotoga* maintained stable correlations with *intI1* across both seasons, suggesting a role in linking flooded–non-flooded transitions and coupling nitrogen cycling with ARG spread [59]. The phase-dependent succession of ARG hosts supports that persistent soil bacteria act as ARG shuttles to maintain resistance gene continuity across contrasting hydrological regimes [60].

3.5. From Carbon to Resistance: An Ecological Cascade Driving ARG Dynamics in Rotated Agroecosystems

RDA, Mantel correlation tests and PLS-SEM collectively demonstrated that soil ARG dynamics in the rice–faba bean rotation systems were governed by multiple environmental factors (Figure 6; full soil physicochemical properties in Supplementary Figure S4 and Table S2; Mantel test statistics summarized in Supplementary Table S3). Among all regulatory pathways resolved by SEM, an indirect multi-tiered cascade centered on soil organic carbon-microbial community-MGEs exerted dominant control over resistome assembly, forming a hierarchically organized, ecologically coherent regulatory framework [1,61]. MGEs had the strongest direct path to ARG abundance in the PLS-SEM (path coefficient = 0.575, $p < 0.001$), placing MGE-associated mobility closest to the observed resistome response. Microbial community structure was negatively associated with MGE abundance (path coefficient = −0.458), suggesting that community turnover altered the size or composition of the mobile genetic element pool. RDA positioned DOC and ROC strongly along the first axis, with loadings of 0.90 and 0.79, while pH loaded in the opposite direction. Mantel tests confirmed highly significant positive correlations between various ARG subtypes and both DOC and ROC, indicating that soil organic carbon availability—particularly active fractions—acted as a core environmental filter regulating microbial community structure and thus the soil resistome [62], indirectly affecting MGE abundances and ultimately driving ARG dynamics via this ecological cascade [63].

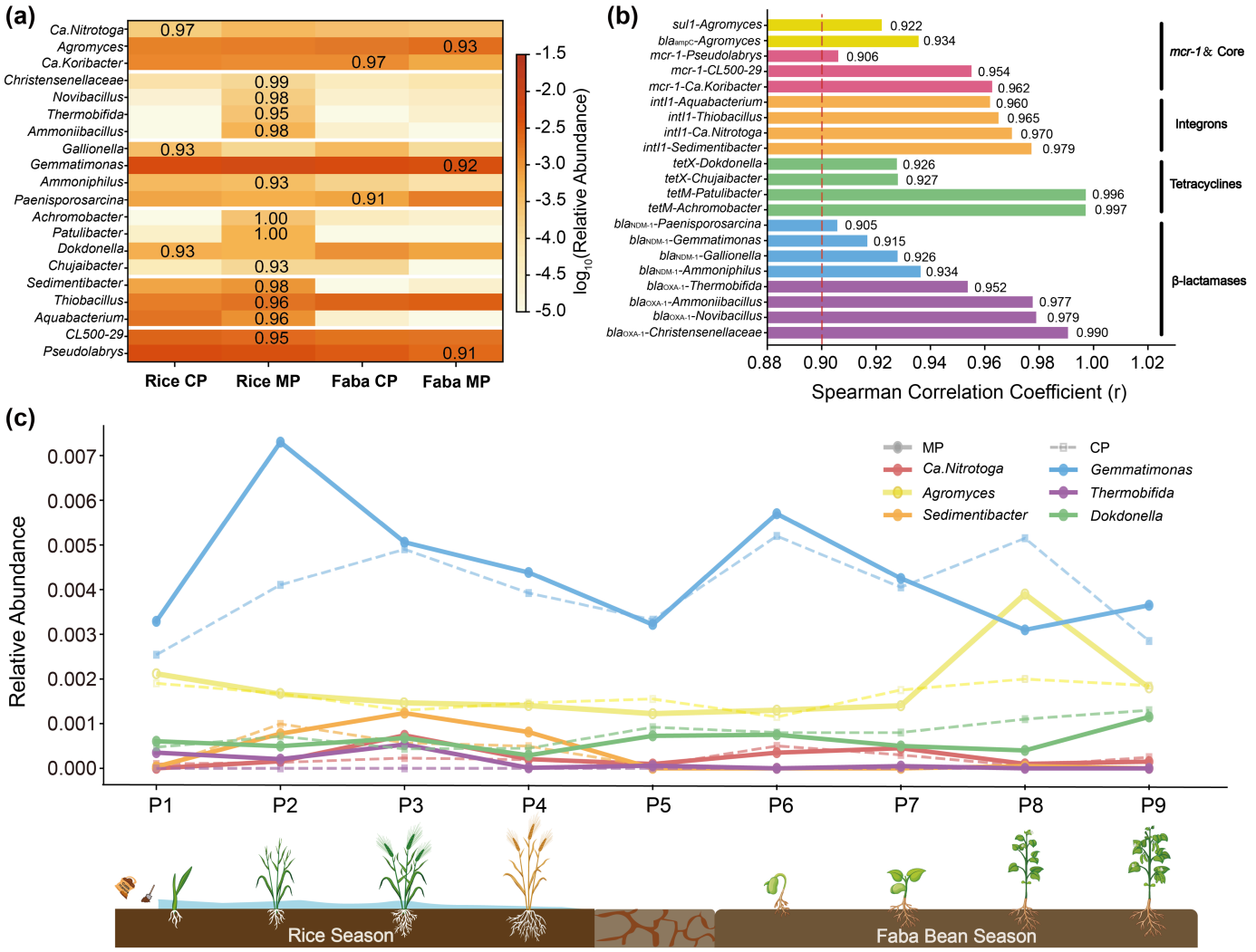


Figure 5. Identification, correlation networks, and temporal dynamics of key potential ARG bacterial hosts. (**a**) Heatmap illustrating the relative abundance of potential ARG host genera across the four treatments (Rice CP, Rice MP, Faba CP, and Faba MP). Values embedded within the heatmap cells denote highly significant positive Spearman correlation coefficients ($r > 0.9$) between the respective hosts and ARGs. (**b**) Specific ARG–host associations grouped by resistance functional categories (*mcr-1* & Core, Integrons, Tetracyclines, and β-lactamases). (**c**) Temporal dynamics of the relative abundance of six representative key host genera across the nine rotation periods (P1–P9).

Beyond this core hierarchical pathway, ARG dynamics are also complexly regulated by other direct and indirect routes. Total effects analysis from the structural equation model showed that hydrological regime exerted the strongest overall negative effect on ARGs, which aligns with recent SEM evaluations emphasizing that agricultural phase transitions in paddy–upland systems fundamentally drive resistome assembly [64], realized through two pathways: direct inhibition of ARGs and indirect regulation via strong promotion of the microbial community, which influenced ARGs through the microbial–MGE pathway. The measured soil enzyme activities, specifically β-glucosidase and sucrase, serve as sensitive bioindicators of soil redox status [65], reflecting the shift from flooded to non-flooded conditions across the rice–faba bean rotation. Successive changes in these enzyme activities revealed that microbial community evolution was closely coupled with variations in soil redox potential. Manure application exhibited an overall positive total effect, but its action pathways were more diverse: it directly inhibits certain soil properties while simultaneously directly promoting enzyme activity and ARGs themselves [66]. The correlation between

glucosidase and various ARGs observed in Mantel tests does not emerge as a direct path in the structural equation model, further supporting that their association may be mediated by shared microbial drivers.

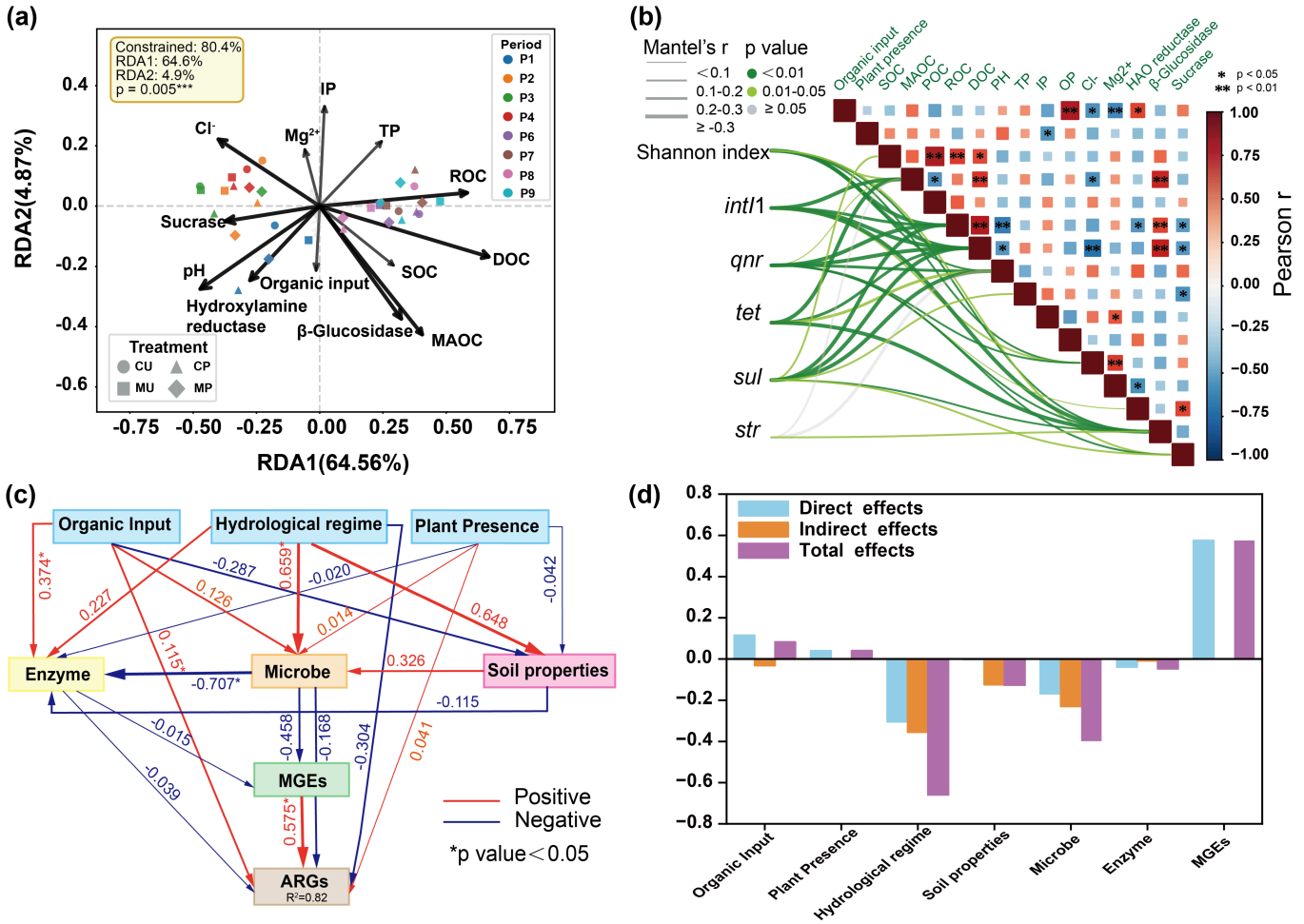


Figure 6. Environmental drivers and mechanistic pathways shaping the soil resistome and microbial community. (**a**) RDA triplot illustrating the relationships between the microbial community structure and environmental variables across different rotation periods (P1–P9) and treatments. (**b**) Mantel test and Pearson correlation heatmap revealing the associations among environmental drivers, microbial alpha diversity (Shannon index), and the relative abundance of major ARG/MGE classes. (**c**) Structural equation model (SEM) depicting the complex direct and indirect effects of agricultural management, soil properties, enzymes, microbial community, and MGEs on the relative abundance of ARGs. Red and blue arrows indicate positive and negative path relationships, respectively. Numbers adjacent to arrows are standardized path coefficients ($p < 0.05$). (**d**) Standardized direct, indirect, and total effects of the corresponding driving factors on ARGs derived from the SEM.

Together, RDA, Mantel tests and PLS-SEM resolved a layered pathway linking hydrological transitions, labile organic carbon, microbial communities, MGEs and ARGs. Hydrological regime and manure altered DOC and ROC, reshaping the microbial setting in which MGEs showed the strongest direct association with ARG abundance. This carbon–microbe–MGE pathway provides a mechanistic explanation for resistome succession. However, different crops may influence ARG dynamics through root growth, nutrient uptake, residue inputs, rhizosphere recruitment, and the release of root-derived metabolites. Future studies should therefore compare multiple crop species under controlled water and fertilization conditions. Integrating plant and rhizosphere metabolomics with

metagenomics and metatranscriptomics could clarify how crop-specific metabolic processes regulate microbial communities, MGEs, and ARG fate.

4. Conclusions

This study demonstrated that the hydrological regime governs the temporal succession of soil resistomes in manure-amended rice–faba bean rotation systems. Across the annual rotation cycle, manure introduced diverse ARGs and MGEs, while cyclic flooded–non-flooded transitions reshaped ARG abundance and composition, with the fallow transition period acting as a critical resistome restructuring window. Multivariate environmental analyses further revealed that active organic carbon fractions, particularly DOC and ROC, were key ecological drivers linking hydrological changes to ARG dynamics. These carbon-mediated effects operated through shifts in microbial community structure and MGE abundance, forming a carbon–microbe–MGE regulatory cascade. Network and host-associated analyses indicated that hydrological transitions reorganized ARG–MGE–bacterial associations, altering potential ARG host assemblages and horizontal gene transfer potential across rotation stages. Collectively, our findings highlight hydrological management and critical transition periods as important targets for mitigating the risk posed by ARGs in manured soil within paddy–upland agroecosystems.

Supplementary Materials: The following supporting information can be downloaded at https://www.mdpi.com/article/10.3390/antibiotics15111052/s1: Text S1: Methods for qPCR assays of the target genes; Table S1: The information of qPCR primers used in this study; Table S2: Soil physicochemical properties across different treatments and sampling periods; Table S3: Mantel test correlations of the soil antibiotic resistome and microbial diversity with environmental properties; Figure S1: Relative abundance of the top 20 bacterial phyla across four treatments (CU, CP, MU, and MP) and nine sampling time points (P1–P9); Figure S2: Temporal successional trajectories of the top five microbial phyla; Figure S3: Relative abundance of the top 20 bacterial genera across four treatments (CU, CP, MU, and MP) and nine sampling time points (P1–P9); Figure S4: Spatiotemporal dynamics of key soil physicochemical properties and enzyme activities. References [67–82] are cited in the Supplementary Materials.

Author Contributions: S.H.: Writing—original draft, Data curation, Visualization. Y.Z. (Ying Zhang): Supervision, Investigation. Y.Z. (Yuanye Zeng): Data curation. S.S.: Formal analysis, Data curation. R.X.: Investigation, Writing—review and editing. K.Z.: Supervision, Project administration. F.Y.: Writing—review and editing, Supervision, Resources, Project administration, Funding acquisition. All authors have read and agreed to the published version of the manuscript.

Funding: This study was financially supported by Yunnan Fundamental Research Projects (202401AT070304), the National Natural Science Foundation of China (42277033), the Youth Innovation Program of the Chinese Academy of Agricultural Sciences (Y2024QC28), and Tianjin Natural Science Foundation Project (23JCYBJC00250).

Institutional Review Board Statement: Not applicable.

Informed Consent Statement: Not applicable.

Data Availability Statement: The original contributions presented in this study are included in the article/Supplementary Material. Further inquiries can be directed to the corresponding authors.

Conflicts of Interest: The authors declare that they have no known competing financial interests or personal relationships that could have appeared to influence the work reported in this paper.

References

1. Zhao, Y.; Li, L.; Huang, Y.; Xu, X.; Liu, Z.; Li, S.; Zhu, L.; Hu, B.; Zhang, T. Global soil antibiotic resistance genes are associated with increasing risk and connectivity to human resistome. *Nat. Commun.* **2025**, *16*, 7141. [CrossRef]
2. Liu, W.; Zhou, W.; Fu, C.; Yu, J.; Hou, G.; Zhang, M.; He, L.; Ding, H. Heavy metals and antibiotic resistance genes in large-scale livestock farming environments: Pollution characteristics, driving factors, and risks to humans. *Biocontaminant* **2025**, *1*, e006. [CrossRef]
3. Zhang, A.-N.; Gaston, J.M.; Dai, C.L.; Zhao, S.; Poyet, M.; Groussin, M.; Yin, X.; Li, L.-G.; van Loosdrecht, M.C.M.; Topp, E.; et al. An omics-based framework for assessing the health risk of antimicrobial resistance genes. *Nat. Commun.* **2021**, *12*, 4765. [CrossRef]
4. Wang, Y.; Sutton, N.B.; Zheng, Y.; Dong, H.; Rijnaarts, H. Effect of wheat crops on the persistence and attenuation of antibiotic resistance genes in soil after swine wastewater application. *J. Hazard. Mater.* **2024**, *468*, 133759. [CrossRef]
5. Cerqueira, F.; Matamoros, V.; Bayona, J.; Elsinga, G.; Hornstra, L.M.; Piña, B. Distribution of antibiotic resistance genes in soils and crops. A field study in legume plants (*Vicia faba* L.) grown under different watering regimes. *Environ. Res.* **2019**, *170*, 16–25. [CrossRef]
6. Shen, Y.; Zhang, B.; Yao, Y.; Wang, H.; Chen, Z.; Hao, A.; Guo, P. Insights into the interactions of plant-associated bacteria and their role in the transfer of antibiotic resistance genes from soil to plant. *J. Hazard. Mater.* **2024**, *480*, 135881. [CrossRef]
7. Davidovich, C.; Erokhina, K.; Gupta, C.L.; Zhu, Y.-G.; Su, J.-Q.; Djordjevic, S.P.; Wyrsch, E.R.; Blum, S.E.; Cytryn, E. Occurrence of "under-the-radar" antibiotic resistance in anthropogenically affected produce. *ISME J.* **2025**, *19*, wrae261. [CrossRef]
8. Castañeda-Barba, S.; Top, E.M.; Stalder, T. Plasmids, a molecular cornerstone of antimicrobial resistance in the One Health era. *Nat. Rev. Microbiol.* **2024**, *22*, 18–32. [CrossRef]
9. Zeng, Y.; Feng, R.; Huang, C.; Liu, J.; Yang, F. Antibiotic resistance genes in agricultural soils: A comprehensive review of the hidden crisis and exploring control strategies. *Toxics* **2025**, *13*, 239. [CrossRef]
10. Zhu, L.; Lian, Y.; Lin, D.; Lin, G.; Wang, M. The profile and persistence of clinically critical antibiotic resistance genes and human pathogenic bacteria in manure-amended farmland soils. *Front. Cell. Infect. Microbiol.* **2022**, *12*, 1073118. [CrossRef]
11. Agga, G.E.; Durso, L.M.; Sistani, K.R. Poultry litter as a soil amendment enriches antibiotic resistant enterococci. *Environ. Pollut.* **2025**, *380*, 126531. [CrossRef]
12. Naghavi, M.; Vollset, S.E.; Ikuta, K.S.; Swetschinski, L.R.; Gray, A.P.; Wool, E.E.; Robles Aguilar, G.; Mestrovic, T.; Smith, G.; Han, C.; et al. Global burden of bacterial antimicrobial resistance 1990–2021: A systematic analysis with forecasts to 2050. *Lancet* **2024**, *404*, 1199–1226. [CrossRef]
13. Xie, W.-Y.; Yuan, S.-T.; Xu, M.-G.; Yang, X.-P.; Shen, Q.-R.; Zhang, W.-W.; Su, J.-Q.; Zhao, F.-J. Long-term effects of manure and chemical fertilizers on soil antibiotic resistome. *Soil Biol. Biochem.* **2018**, *122*, 111–119. [CrossRef]
14. Xu, Y.; Zhang, D.; Li, H.; Ye, H.; Bai, M.; Jiang, G.; Li, X. Unraveling the determinants of antibiotic resistance evolution in farmland under fertilizations. *J. Hazard. Mater.* **2024**, *474*, 134802. [CrossRef]
15. Xiang, Q.; Fu, C.-X.; Lu, C.-Y.; Sun, A.-Q.; Chen, Q.-L.; Qiao, M. Flooding drives the temporal turnover of antibiotic resistance gene in manure-amended soil–water continuum. *Environ. Int.* **2023**, *179*, 108168. [CrossRef]
16. Iheshiulo, E.M.-A.; Larney, F.J.; Hernandez-Ramirez, G.; Luce, M.S.; Liu, K.; Chau, H.W. Do diversified crop rotations influence soil physical health? A meta-analysis. *Soil Tillage Res.* **2023**, *233*, 105781. [CrossRef]
17. Badri, D.V.; Vivanco, J.M. Regulation and function of root exudates. *Plant Cell Environ.* **2009**, *32*, 666–681. [CrossRef]
18. Bi, B.; Wang, K.; Zhang, H.; Wang, Y.; Fei, H.; Pan, R.; Han, F. Plants use rhizosphere metabolites to regulate soil microbial diversity. *Land Degrad. Dev.* **2021**, *32*, 5267–5280. [CrossRef]
19. Yang, J.; Lan, L.; Jin, Y.; Yu, N.; Wang, D.; Wang, E. Mechanisms underlying legume–rhizobium symbioses. *J. Integr. Plant Biol.* **2022**, *64*, 244–267. [CrossRef]
20. Zheng, H.; Huang, H.; Zhang, C.; Li, J. National-scale paddy-upland rotation in Northern China promotes sustainable development of cultivated land. *Agric. Water Manag.* **2016**, *170*, 20–25. [CrossRef]
21. Yin, X.; Li, Q.; Zhang, X.; Wang, Z.; Li, Q.; Wei, L.; Huang, T.; Gao, M. Paddy–upland rotation improves rice growth and reduces greenhouse gas emissions in winter paddy fields. *Agronomy* **2025**, *15*, 349. [CrossRef]
22. Wang, P.; Wang, B.; Chen, A.; Sun, X.; Du, C.; Zhu, H.; Pan, Y.; Tang, L. Organic substitution accumulates more nitrogen in soil while maintaining unchanged nitrogen use efficiency in rice-fava bean rotation system. *Land Degrad. Dev.* **2023**, *34*, 5416–5429. [CrossRef]
23. Wei, L.; Ge, T.; Zhu, Z.; Ye, R.; Peñuelas, J.; Li, Y.; Lynn, T.M.; Jones, D.L.; Wu, J.; Kuzyakov, Y. Paddy soils have a much higher microbial biomass content than upland soils: A review of the origin, mechanisms, and drivers. *Agric. Ecosyst. Environ.* **2022**, *326*, 107798. [CrossRef]
24. FAO. *Standard Operating Procedure for Soil pH Determination*; GLOSOLAN-SOP-06; Food and Agriculture Organization of the United Nations: Rome, Italy, 2021; p. 23.

25. FAO. *Standard Operating Procedure for Soil Organic Carbon. Walkley-Black Method: Titration and Colorimetric Method*; GLOSOLAN-SOP-02; Food and Agriculture Organization of the United Nations: Rome, Italy, 2019; p. 27.
26. Wade, J.; Maltais-Landry, G.; Lucas, D.E.; Bongiorno, G.; Bowles, T.M.; Calderón, F.J.; Culman, S.W.; Daughtridge, R.; Ernakovich, J.G.; Fonte, S.J.; et al. Assessing the sensitivity and repeatability of permanganate oxidizable carbon as a soil health metric: An interlab comparison across soils. *Geoderma* **2020**, *366*, 114235. [CrossRef]
27. Wu, H.; Lu, X.; Tong, S.; Batzer, D.P. Soil engineering ants increase CO2 and N2O emissions by affecting mound soil physicochemical characteristics from a marsh soil: A laboratory study. *Appl. Soil Ecol.* **2015**, *87*, 19–26. [CrossRef]
28. Margenot, A.J.; Nakayama, Y.; Parikh, S.J. Methodological recommendations for optimizing assays of enzyme activities in soil samples. *Soil Biol. Biochem.* **2018**, *125*, 350–360. [CrossRef]
29. Zhang, R.; Zhang, H.; Yang, C.; Li, H.; Wu, J. Effects of water stress on nutrients and enzyme activity in rhizosphere soils of greenhouse grape. *Front. Microbiol.* **2024**, *15*, 1376849. [CrossRef]
30. Gikonyo, F.N.; Dong, X.; Mosongo, P.S.; Guo, K.; Liu, X. Long-term impacts of different cropping patterns on soil physico-chemical properties and enzyme activities in the low land plain of North China. *Agronomy* **2022**, *12*, 471. [CrossRef]
31. Du, Z.; Wang, X.; Xiang, J.; Wu, Y.; Zhang, B.; Yan, Y.; Zhang, X.; Cai, Y. Yak dung pat fragmentation affects its carbon and nitrogen leaching in Northern Tibet, China. *Agric. Ecosyst. Environ.* **2021**, *310*, 107301. [CrossRef]
32. Tang, X.; Chen, Y.; Dai, Z.; Chang, S.X.; Zeng, R.; He, D.; Xu, J. Multiple environmental stressors interactively affect soil phosphorus cycling microbiomes. *Commun. Earth Environ.* **2025**, *6*, 757. [CrossRef]
33. Zhou, X.; Liu, X.; Liu, M.; Liu, W.; Xu, J.; Li, Y. Comparative evaluation of 16S rRNA primer pairs in identifying nitrifying guilds in soils under long-term organic fertilization and water management. *Front. Microbiol.* **2024**, *15*, 1424795. [CrossRef]
34. Bolyen, E.; Rideout, J.R.; Dillon, M.R.; Bokulich, N.A.; Abnet, C.C.; Al-Ghalith, G.A.; Alexander, H.; Alm, E.J.; Arumugam, M.; Asnicar, F.; et al. Reproducible, interactive, scalable and extensible microbiome data science using QIIME 2. *Nat. Biotechnol.* **2019**, *37*, 852–857. [CrossRef]
35. Martin, M. Cutadapt removes adapter sequences from high-throughput sequencing reads. *EMBnet. J.* **2011**, *17*, 10–12. [CrossRef]
36. Callahan, B.J.; McMurdie, P.J.; Rosen, M.J.; Han, A.W.; Johnson, A.J.A.; Holmes, S.P. DADA2: High-resolution sample inference from Illumina amplicon data. *Nat. Methods* **2016**, *13*, 581–583. [CrossRef]
37. Bokulich, N.A.; Kaehler, B.D.; Rideout, J.R.; Dillon, M.; Bolyen, E.; Knight, R.; Huttley, G.A.; Gregory Caporaso, J. Optimizing taxonomic classification of marker-gene amplicon sequences with QIIME 2's q2-feature-classifier plugin. *Microbiome* **2018**, *6*, 90. [CrossRef]
38. Quast, C.; Pruesse, E.; Yilmaz, P.; Gerken, J.; Schweer, T.; Yarza, P.; Peplies, J.; Glöckner, F.O. The SILVA ribosomal RNA gene database project: Improved data processing and web-based tools. *Nucleic Acids Res.* **2013**, *41*, D590–D596. [CrossRef]
39. Zheng, J.; Li, Y.-Y.; Lu, Y.-S.; Wang, D.; Liu, C.; Peng, H.-L.; Shi, C.-H.; Xie, K.-Z.; Zhang, K.; Sun, L.-L.; et al. Impact of different continuous fertilizations on the antibiotic resistome associated with a subtropical triple-cropping system over one decade. *Environ. Pollut.* **2025**, *367*, 125564. [CrossRef]
40. Wind, L.; Krometis, L.-A.; Hession, W.C.; Pruden, A. Cross-comparison of methods for quantifying antibiotic resistance in agricultural soils amended with dairy manure and compost. *Sci. Total Environ.* **2021**, *766*, 144321. [CrossRef]
41. Liu, Z.-T.; Ma, R.-A.; Zhu, D.; Konstantinidis, K.T.; Zhu, Y.-G.; Zhang, S.-Y. Organic fertilization co-selects genetically linked antibiotic and metal(loid) resistance genes in global soil microbiome. *Nat. Commun.* **2024**, *15*, 5168. [CrossRef]
42. Han, B.; Yang, F.; Shen, S.; Mu, M.; Zhang, K. Effects of soil habitat changes on antibiotic resistance genes and related microbiomes in paddy fields. *Sci. Total Environ.* **2023**, *895*, 165109. [CrossRef]
43. Ruiz-Torrubia, F.; Garbisu, C.; Gómez-Sagasti, M.T.; Artetxe, U.; Becerril, J.M.; Epelde, L. Impacts of drought and manure fertilization on soil and radish resistomes. *Sci. Rep.* **2026**, *16*, 10621. [CrossRef]
44. Jiang, C.; Zhao, Z.; Zhu, D.; Pan, X.; Yang, Y. Rare resistome rather than core resistome exhibited higher diversity and risk along the Yangtze River. *Water Res.* **2024**, *249*, 120911. [CrossRef]
45. Sao, S.; Praise, S.; Nishiyama, M.; Ann, V.; Phung, L.D.; Watanabe, T. Response of bacterial communities and soil chemistry to flood durations and recovery phases. *Environ. Sci. Pollut. Res.* **2025**, *32*, 9429–9442. [CrossRef]
46. Abdallah, R.Z.; Wegner, C.-E.; Liesack, W. Community transcriptomics reveals drainage effects on paddy soil microbiome across all three domains of life. *Soil Biol. Biochem.* **2019**, *132*, 131–142. [CrossRef]
47. Delgado-Baquerizo, M.; Hu, H.-W.; Maestre, F.T.; Guerra, C.A.; Eisenhauer, N.; Eldridge, D.J.; Zhu, Y.-G.; Chen, Q.-L.; Trivedi, P.; Du, S.; et al. The global distribution and environmental drivers of the soil antibiotic resistome. *Microbiome* **2022**, *10*, 219. [CrossRef]
48. van der Meij, A.; Worsley, S.F.; Hutchings, M.I.; van Wezel, G.P. Chemical ecology of antibiotic production by actinomycetes. *FEMS Microbiol. Rev.* **2017**, *41*, 392–416. [CrossRef]
49. Wang, G.; Gao, X.; Cai, Y.; Li, G.; Ma, R.; Yuan, J. Dynamics of antibiotic resistance genes during manure composting: Reduction in herbivores manure and accumulation in carnivores. *Environ. Int.* **2024**, *190*, 108900. [CrossRef]

50. Zheng, D.; Yin, G.; Liu, M.; Hou, L.; Yang, Y.; Van Boeckel, T.P.; Zheng, Y.; Li, Y. Global biogeography and projection of soil antibiotic resistance genes. *Sci. Adv.* **2022**, *8*, eabq8015. [CrossRef]
51. Redondo-Salvo, S.; Fernández-López, R.; Ruiz, R.; Vielva, L.; de Toro, M.; Rocha, E.P.C.; Garcillán-Barcia, M.P.; de la Cruz, F. Pathways for horizontal gene transfer in bacteria revealed by a global map of their plasmids. *Nat. Commun.* **2020**, *11*, 3602. [CrossRef]
52. Qiao, M.; Sun, R.; Wang, Z.; Dumack, K.; Xie, X.; Dai, C.; Wang, E.; Zhou, J.; Sun, B.; Peng, X.; et al. Legume rhizodeposition promotes nitrogen fixation by soil microbiota under crop diversification. *Nat. Commun.* **2024**, *15*, 2924. [CrossRef]
53. Li, G.; Niu, W.; Ma, L.; Du, Y.; Zhang, Q.; Sun, J.; Siddique, K.H.M. Legacy effects of wheat season organic fertilizer addition on microbial co-occurrence networks, soil function, and yield of the subsequent maize season in a wheat-maize rotation system. *J. Environ. Manag.* **2023**, *347*, 119160. [CrossRef]
54. Xu, M.; Wang, F.; Sheng, H.; Stedtfeld, R.D.; Li, Z.; Hashsham, S.A.; Jiang, X.; Tiedje, J.M. Does anaerobic condition play a more positive role in dissipation of antibiotic resistance genes in soil? *Sci. Total Environ.* **2021**, *757*, 143737. [CrossRef]
55. Yu, F.; Zhang, Y.; Wen, Y.; Peng, Z.; Xu, D.; Xiao, J. Divergent risk gene profiles in smallholder and large-scale paddy farms. *Environ. Res.* **2025**, *285*, 122406. [CrossRef]
56. Ibekwe, A.M.; Bhattacharjee, A.S.; Phan, D.; Ashworth, D.; Schmidt, M.P.; Murinda, S.E.; Obayiuwana, A.; Murry, M.A.; Schwartz, G.; Lundquist, T.; et al. Potential reservoirs of antimicrobial resistance in livestock waste and treated wastewater that can be disseminated to agricultural land. *Sci. Total Environ.* **2023**, *872*, 162194. [CrossRef]
57. Liu, Y.-Y.; Wang, Y.; Walsh, T.R.; Yi, L.-X.; Zhang, R.; Spencer, J.; Doi, Y.; Tian, G.; Dong, B.; Huang, X.; et al. Emergence of plasmid-mediated colistin resistance mechanism MCR-1 in animals and human beings in China: A microbiological and molecular biological study. *Lancet Infect. Dis.* **2016**, *16*, 161–168. [CrossRef]
58. Gillings, M.R. Integrons: Past, present, and future. *Microbiol. Mol. Biol. Rev.* **2014**, *78*, 257–277. [CrossRef]
59. Wang, Y.; Cai, J.; Chen, X.; Guo, B.; Liu, J.; Qiu, G.; Li, H. The connection between the antibiotic resistome and nitrogen-cycling microorganisms in paddy soil is enhanced by application of chemical and plant-derived organic fertilizers. *Environ. Res.* **2024**, *243*, 117880. [CrossRef]
60. Yu, T.; Huang, Y.; Zhang, Y.; Wang, S.; Wang, X.; Jiang, Y.; Zang, H.; Zeng, Z.; Yang, Y. Manure input propagated antibiotic resistance genes and virulence factors in soils by regulating microbial carbon metabolism. *Environ. Pollut.* **2025**, *375*, 126293. [CrossRef]
61. Bengtsson-Palme, J.; Kristiansson, E.; Larsson, D.G.J. Environmental factors influencing the development and spread of antibiotic resistance. *FEMS Microbiol. Rev.* **2018**, *42*, fux053. [CrossRef]
62. Zhou, J.; Deng, Y.; Shen, L.; Wen, C.; Yan, Q.; Ning, D.; Qin, Y.; Xue, K.; Wu, L.; He, Z.; et al. Temperature mediates continental-scale diversity of microbes in forest soils. *Nat. Commun.* **2016**, *7*, 12083. [CrossRef]
63. Ding, J.; Zhu, D.; Hong, B.; Wang, H.T.; Li, G.; Ma, Y.B.; Tang, Y.T.; Chen, Q.L. Long-term application of organic fertilization causes the accumulation of antibiotic resistome in earthworm gut microbiota. *Environ. Int.* **2019**, *124*, 145–152. [CrossRef]
64. Han, B.; Shen, S.; Yang, F.; Wang, X.; Gao, W.; Zhang, K. Exploring antibiotic resistance load in paddy-upland rotation fields amended with commercial organic and chemical/slow release fertilizer. *Front. Microbiol.* **2023**, *14*, 1184238. [CrossRef]
65. Wang, C.; Blagodatskaya, E.; Dippold, M.A.; Dorodnikov, M. Keep oxygen in check: Contrasting effects of short-term aeration on hydrolytic versus oxidative enzymes in paddy soils. *Soil Biol. Biochem.* **2022**, *169*, 108690. [CrossRef]
66. Zhang, Y.-J.; Hu, H.-W.; Chen, Q.-L.; Singh, B.K.; Yan, H.; Chen, D.; He, J.-Z. Transfer of antibiotic resistance from manure-amended soils to vegetable microbiomes. *Environ. Int.* **2019**, *130*, 104912. [CrossRef]
67. Aminov, R.I.; Garrigues-Jeanjean, N.; Mackie, R.I. Molecular ecology of tetracycline resistance: Development and validation of primers for detection of tetracycline resistance genes encoding ribosomal protection proteins. *Appl. Environ. Microbiol.* **2001**, *67*, 22–32. [CrossRef]
68. Chen, B.; He, R.; Yuan, K.; Chen, E.; Lin, L.; Chen, X.; Sha, S.; Zhong, J.; Lin, L.; Yang, L.; et al. Polycyclic aromatic hydrocarbons (PAHs) enriching antibiotic resistance genes (ARGs) in the soils. *Environ. Pollut.* **2017**, *220*, 1005–1013. [CrossRef]
69. Ghigo, J.-M. Natural conjugative plasmids induce bacterial biofilm development. *Nature* **2001**, *412*, 442–445. [CrossRef]
70. Goldstein, C.; Lee, M.D.; Sanchez, S.; Hudson, C.; Phillips, B.; Register, B.; Grady, M.; Liebert, C.; Summers, A.O.; White, D.G.; et al. Incidence of class 1 and 2 integrases in clinical and commensal bacteria from livestock, companion animals, and exotics. *Antimicrob. Agents Chemother.* **2001**, *45*, 723–726. [CrossRef]
71. Kim, H.B.; Wang, M.; Park, C.H.; Kim, E.-C.; Jacoby, G.A.; Hooper, D.C. oqxAB encoding a multidrug efflux pump in human clinical isolates of Enterobacteriaceae. *Antimicrob. Agents Chemother.* **2009**, *53*, 3582–3584. [CrossRef]
72. Li, H.; Zheng, X.; Tan, L.; Shao, Z.; Cao, H.; Xu, Y. The vertical migration of antibiotic-resistant genes and pathogens in soil and vegetables after the application of different fertilizers. *Environ. Res.* **2022**, *203*, 111884. [CrossRef]
73. Luo, Y.; Yang, F.; Mathieu, J.; Mao, D.; Wang, Q.; Alvarez, P.J.J. Proliferation of multidrug-resistant New Delhi metallo-β-lactamase genes in municipal wastewater treatment plants in Northern China. *Environ. Sci. Technol. Lett.* **2014**, *1*, 26–30. [CrossRef]

74. Mu, Q.; Li, J.; Sun, Y.; Mao, D.; Wang, Q.; Luo, Y. Occurrence of sulfonamide-, tetracycline-, plasmid-mediated quinolone- and macrolide-resistance genes in livestock feedlots in Northern China. *Environ. Sci. Pollut. Res.* **2015**, *22*, 6932–6940. [CrossRef]
75. Pei, R.; Kim, S.-C.; Carlson, K.H.; Pruden, A. Effect of river landscape on the sediment concentrations of antibiotics and corresponding antibiotic resistance genes (ARG). *Water Res.* **2006**, *40*, 2427–2435. [CrossRef]
76. Suzuki, M.T.; Taylor, L.T.; DeLong, E.F. Quantitative analysis of small-subunit rRNA genes in mixed microbial populations via 5′-nuclease assays. *Appl. Environ. Microbiol.* **2000**, *66*, 4605–4614. [CrossRef]
77. Walsh, F.; Ingenfeld, A.; Zampicolli, M.; Hilber-Bodmer, M.; Frey, J.E.; Duffy, B. Real-time PCR methods for quantitative monitoring of streptomycin and tetracycline resistance genes in agricultural ecosystems. *J. Microbiol. Methods* **2011**, *86*, 150–155. [CrossRef]
78. Wang, J.; Mao, D.; Mu, Q.; Luo, Y. Fate and proliferation of typical antibiotic resistance genes in five full-scale pharmaceutical wastewater treatment plants. *Sci. Total Environ.* **2015**, *526*, 366–373. [CrossRef]
79. Wang, M.; Sun, Y.; Liu, P.; Sun, J.; Zhou, Q.; Xiong, W.; Zeng, Z. Fate of antimicrobial resistance genes in response to application of poultry and swine manure in simulated manure-soil microcosms and manure-pond microcosms. *Environ. Sci. Pollut. Res.* **2017**, *24*, 20949–20958. [CrossRef]
80. Xu, Y.; Xu, J.; Mao, D.; Luo, Y. Effect of the selective pressure of sub-lethal level of heavy metals on the fate and distribution of ARGs in the catchment scale. *Environ. Pollut.* **2017**, *220*, 900–908. [CrossRef]
81. Yang, F.; Zhang, K.; Zhi, S.; Li, J.; Tian, X.; Gu, Y.; Zhou, J. High prevalence and dissemination of β-lactamase genes in swine farms in northern China. *Sci. Total Environ.* **2019**, *651*, 2507–2513. [CrossRef]
82. You, Y.; Hilpert, M.; Ward, M.J. Detection of a Common and Persistent tet(L)-Carrying Plasmid in Chicken-Waste-Impacted Farm Soil. *Appl. Environ. Microbiol.* **2012**, *78*, 3203–3213. [CrossRef]

Disclaimer/Publisher's Note: The statements, opinions and data contained in all publications are solely those of the individual author(s) and contributor(s) and not of MDPI and/or the editor(s). MDPI and/or the editor(s) disclaim responsibility for any injury to people or property resulting from any ideas, methods, instructions or products referred to in the content.